# Optical model for low-energy neutrons on $^{60}$Ni

R. R. Winters
*Denison University, Granville, Ohio 43023*

C. H. Johnson
*Oak Ridge National Laboratory, Oak Ridge, Tennessee 37831*

A. D. MacKellar
*University of Kentucky, Lexington, Kentucky 40506*

(Received 28 September 1984)

A previously published $s$-wave scattering function for 1—450 keV neutrons on $^{60}$Ni is averaged for comparison to the scattering from an optical model potential. The scattering length $R'$ is found to be 5.5±0.03 fm at 225 keV. Averaging of the scattering function (both by integration with a normalized weight function and by use of an analytical approximation) produces shape elastic and compound nucleus cross sections which are then fitted by adjustment of the real and imaginary well depths in both spherical and vibrational optical models with a Woods-Saxon real well ($r_0=1.21$ fm, $a_0=0.66$ fm) and a surface derivative imaginary well ($r_D=1.21$ fm, $a_D=0.48$ fm). The fitted depths are $V_0=48$ MeV and $W_D=29$ MeV for the spherical potentials, and $V_0=50$ MeV and $W_D=24$ MeV for the vibrational potentials. Uncertainties are ±5 MeV. From an upper limit on the $p$-wave strength function the $W_D$ for $p$ waves is found to be 1.5 MeV for the vibrational model. Thus, the imaginary potential is $l$ dependent for the assumed geometry. For $s$ waves the vibrational model gives a good fit also with $W_D=1.5$ MeV and $V_0=54.4$ MeV; however, with that $V_0$ the $2p$ states are bound too deeply in $^{61}$Ni and the $3s$ size resonance is predicted at too low a mass.

## I. INTRODUCTION

For many years a fruitful application of the phenomenological optical model potential (OMP) has been to the scattering of neutrons at only a few keV, where $s$ waves dominate. Thereby OMP parameters have been deduced specifically for $s$ waves over a broad mass region. The comparison between the OMP scattering function and the average experimental scattering function for $s$ waves has involved two experimental quantities. One is the strength function $S_0=\langle\Gamma_n^0\rangle/D$, which is the average $s$-wave neutron resonance reduced width per energy interval, and is closely related to the imaginary part of the OMP. The other is the potential scattering length $R'$, which is found from the off-resonance scattering and is closely related to the real part of the OMP. Tabulations[1] of these quantities are available.

Since early measurements were made over small energy regions with few resonances, both $S_0$ and $R'$ had inherent uncertainties due to the fluctuations in the widths and spacings of the resonances. A meaningful comparison to the OMP required data for several neighboring nuclei. For medium weight and lighter nuclei these uncertainties can be reduced by extending the measurements with good resolution to several hundred keV. A careful multilevel analysis is then required to isolate the $s$ waves from higher partial waves. Here we evaluate in terms of the OMP the recent high resolution data for 1 to 450 keV neutrons on $^{60}$Ni which Perey *et al.*[2] obtained and analyzed at the Oak Ridge Electron Linear Accelerator (ORELA). For $s$ waves their analysis gives small uncertainties not only for $S_0$, because many levels are observed, but also for the off-resonance parameters, because for most of the region of measurement the outer levels are far away relative to their spacings. Given these uncertainties the comparison to the OMP becomes meaningful even for this single nucleus.

To deduce an OMP from high resolution cross sections requires that the $R$-matrix scattering function be averaged for comparison to the OMP function. The quantities $R'$ and $S_0$ do give that average, but only at low energies. In fact, $R'$ is usually defined in the zero-energy limit

$$R'=\lim_{E\to 0}\frac{\text{Real}\,\delta}{k}\,, \tag{1}$$

where $\delta$ is the phase shift for the OMP scattering function and $k$ is the neutron wave number. The $S_0$ is not so limited, but it is not precisely defined at higher energies because it depends on the arbitrary radius that is chosen for the multilevel analysis. This problem of averaging the scattering function over a larger energy region was treated recently by Johnson, Larson, Mahaux, and Winters (JLMW) (Ref. 3). Using a normalized weighting function they averaged an experimental scattering function by straightforward numerical integration and then showed that an acceptable description of this average is achieved by a simple analytic approximation.

We follow the procedure of JLMW but note that MacDonald and Birse[4] defined the average to be the parametrized scattering function evaluated at the complex energy $E+iI$, with $2I$ being the width of a Lorentzian function. They then compared the average thus defined

 

to the OMP scattering function calculated at the same complex energy. JLMW examined and rejected that expression for the averaging. Further discussion of these discrepant definitions are presented in a Comment[5] and a Reply[6] by the authors of the original papers.[3,4]

Following JLMW we calculate the average both by the numerical integration and by the analytic approximation and find good agreement between the two. As JLMW stated, the resulting averages can be presented in various forms for comparison to the OMP scattering function. We plot the shape elastic and compound nuclear cross sections, $\sigma_{se}$ and $\sigma_c$, both of which are independent of boundary conditions. The $\sigma_c$ is related to $S_0$ and $\sigma_{se}$ is related to $R'$. Such cross sections were plotted also by Johnson and Winters[7] for neutrons on $^{32}$S and by Carlton *et al.*[8] for $^{30}$Si and $^{34}$S. Alternatively, we could present a complex phase shift $\delta$. In fact, we do plot $\mathrm{Re}(\delta/k)$ to show the relation to the traditional $R'$.

In Sec. II we review the averaging procedures of JLMW and apply them to the data for $s$ waves on $^{60}$Ni by Perey *et al.* In Sec. III we describe the resulting compound and shape elastic cross sections with both a spherical and a vibrational OMP. In Sec. IV we present results also in terms of $R'$. Section V is an extension to the limited data on $p$ waves. In Sec. VI we discuss total cross section measurements[9,10] and compare our low energy optical model with one obtained by the group[11] at Duke University. Section VII is a discussion with conclusions.

## II. AVERAGING OF THE EXPERIMENTAL SCATTERING FUNCTION

Perey *et al.*[2] parametrized the $s$-wave scattering function for n + $^{60}$Ni using the $R$-matrix formalism,

$$S_p(E)=e^{-2i\phi(E)}\frac{1+iP(E)R(E)}{1-iP(E)R(E)}\ , \tag{2}$$

where $\phi$ is the hard-sphere phase shift at their chosen boundary radius of 6 fm, $P$ is the corresponding penetrability, and the $R$ function is a sum over the observed $s$-wave levels plus a smoothly increasing function $R^{\mathrm{ext}}$ that accounts for the effects of levels outside the measured region. The solid curve in Fig. 1 shows their $R^{\mathrm{ext}}$, which they determined to better than $\pm 2\%$ throughout the interval.

From the 30 observed $s$-wave resonances they determined the strength function $S_0$ to $\pm 25\%$. For our purposes we write this strength in different units,

$$\tilde{s}_0 \equiv \langle \gamma^2 \rangle / D = \frac{\Sigma_N \gamma_\lambda^2 / N}{(E_N - E_1)/(N-1)}$$

$$= 0.092 \pm 0.024\ . \tag{3}$$

The two are proportional,

$$S_0 = 4.39\ \mathrm{fm}^{-1} \times 10^{-4} \tilde{s}_0 a A/(A+1)\ , \tag{4}$$

where $A$ is the target mass and $a$ is the boundary radius in fm. (For simplicity in writing the following equations the subscript denoting the partial wave is omitted.)

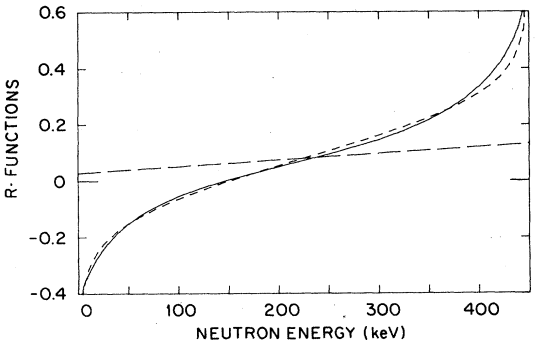


FIG. 1. Smooth $R$ function for $s$-wave neutrons on $^{60}$Ni: solid curve is $R^{\mathrm{ext}}$ from Ref. 2, short-dash curve is the fit by Eq.(5), and long-dash curve is $\tilde{R}$ from Eq. (6).

In preparation for averaging by the analytic approximation of JLMW, we first parametrize $R^{\mathrm{ext}}$ by the expression

$$R^{\mathrm{ext}}(E)=\tilde{R}(E)-\tilde{s}\ln\frac{E_u-E}{E-E_l}\ , \tag{5}$$

where $E_l$ and $E_u$ are the lower and upper energy limits of the data, and where $\tilde{R}$ is a parametric function to be used to fit $R^{\mathrm{ext}}$. We use a linear form,

$$\tilde{R}(E)=\alpha+\beta(E-E_m)\ , \tag{6}$$

where $E_m$ is the midpoint (225 keV) of the measurements. By least squares adjustment we obtained the fit shown by the dashed curve in Fig. 1 with the parameters $\alpha=0.081\pm0.006$ and $\beta=0.23\pm0.32$ MeV$^{-1}$. The large uncertainty in $\beta$ is propagated from the $\pm 25\%$ statistical uncertainty in $\tilde{s}$. The approximate average is given by the expression

$$S^{\mathrm{OM}}(E)=e^{-2i\phi(E)}\frac{1+iP(E)[\tilde{R}(E)+i\pi\tilde{s}+R^f(E+iI)]}{1-iP(E)[\tilde{R}(E)+i\pi\tilde{s}+R^f(E+iI)]}\ . \tag{7}$$

The function $R^f$ [see Eq. (8) of Ref. 8] fluctuates with energy due to the variation of widths and spacings of the resonances, but goes toward zero as the width $2I$ of the averaging function becomes large. Here we choose $2I=180$ keV, or about 12 times the average level spacing $D$. In Fig. 2 the solid curves show the resulting boundary-independent cross sections, $\sigma_c$ and $\sigma_{se}$. Typical uncertainties are shown by vertical bars.

We also averaged by numerical integration to check the above-mentioned approximation. As JLMW stated, it is in the spirit of the optical model to average the variations of the scattering function about a smooth background. Therefore we factor $S_p(E)$ into resonant and background terms and calculate the average defined by

$$S^{\mathrm{OM}}(E)=S_{\mathrm{bkg}}(E)\langle S_{\mathrm{res}}(E)\rangle_I\ . \tag{8}$$

For the foregoing parametrization we have

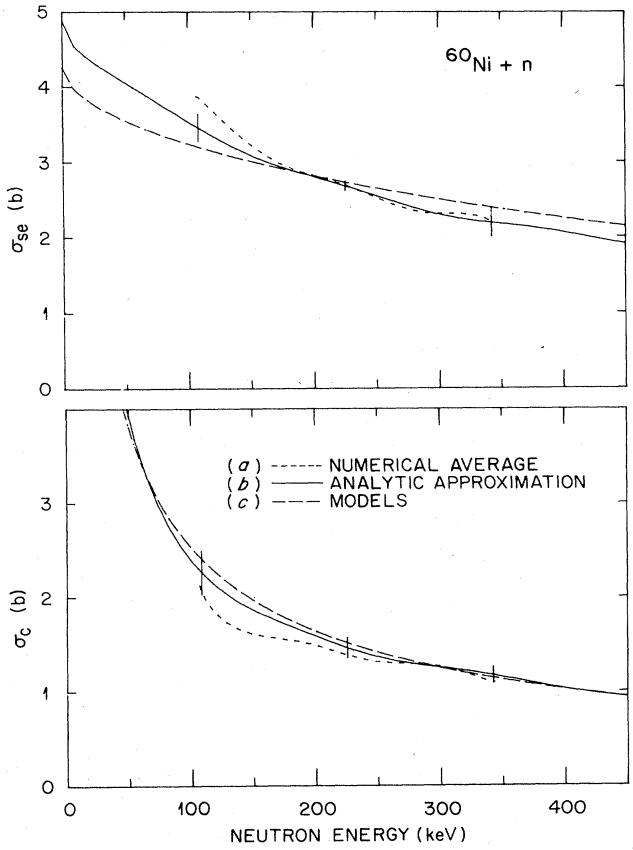


FIG. 2. Compound and shape elastic cross sections for $s$-wave neutrons on $^{60}$Ni. For $2I=180$ keV the numerical average is from Eqs. (8)—(12) plotted vs $\bar{E}$ and the analytical approximation is from Eq. (7) plotted vs $E$. The model is either the coupled channel or spherical OMP with geometry of $r_0=r_D=1.21$ fm, $a_0=0.66$ fm, and $a_D=0.48$ fm.

$$S_{\rm bkg}(E)=e^{-2i\phi(E)}\frac{1+iP(E)\tilde{R}(E)}{1-iP(E)\tilde{R}(E)} \tag{9}$$

and

$$S_{\rm res}(E)=S_p(E)/S_{\rm bkg}(E)\ . \tag{10}$$

This parametrization of $S_{\rm bkg}$ is convenient but not essential; the numerical averaging is insensitive to the particular parametrization. The average of $S_{\rm res}$ is defined by

$$\langle S_{\rm res}(\bar{E})\rangle_I=\int_{E_l}^{E_u}F_I(E,E')S_{\rm res}(E')dE'\ , \tag{11}$$

where $F_I$ is a weighting function normalized in the region,

$$\int_{E_l}^{E_u}F_I(E,E')dE'=1\ , \tag{12}$$

and $\bar{E}$ is the averaged energy found by replacing $S_{\rm res}$ by $E'$ in Eq. (11). Here we use a Lorentzian function

$$F_I(E,E')=f_I[(E-E')^2+I^2]^{-1}\ , \tag{13}$$

where $f_I$ satisfies the normalization. The resulting numerical average for $2I=180$ keV is plotted vs $\bar{E}$ in Fig. 2. Indeed Eq. (7) is a good approximation.

## III. SPHERICAL AND COUPLED CHANNEL OMP FOR $s$ WAVES

Modern models have many parameters, but the present data on $\sigma_c$ and $\sigma_{se}$ can determine only two quantities which are, qualitatively, the volume integrals of the real and imaginary parts of the OMP. Thus only two appropriate parameters can be free. To facilitate comparison with the recent work[7,8] on $^{30}$Si, $^{32}$S, and $^{34}$S, we use the same potential geometry, namely a real Woods-Saxon well plus a surface derivative spin-orbit term with $r_0=1.21$ fm and $a_0=0.66$ fm and a surface-derivative imaginary form with $r_D=1.21$ fm and $a_D=0.48$ fm. We assume $V_{so}=5$ MeV for the spin-orbit potential; it has no consequence for $s$ waves in a spherical well, but enters into the coupled-channel model. The remaining two adjustable parameters are the real and imaginary well depths, $V_0$ and $W_D$.

In Fig. 2 the long-dash curves show the best fits achieved by adjustment of the well depths for a spherical OMP. The fitting required minimizing a $\chi^2$ with weights given by the inverse squares of the experimental uncertainties. Table I lists not only the best fit well depths (sph) with uncertainties but also, for comparison, the parameters deduced previously[7,8] for $^{30}$Si, $^{32}$S, and $^{34}$S. The real well depth $V_0$ is consistent with other nuclei, but the imaginary well depth $W_D$ is quite large, at 29 MeV.

The spherical model could be a poor approximation because $^{60}$Ni is a vibrational nucleus. Therefore, we repeated the fit using the coupled-channel formalism,[12,13] just as MacKellar and Castel[14,15] did earlier for $^{30}$Si, $^{32}$S, and $^{34}$S. Here the target channels are the $0^+$ ground state and the $2^+$ state at 1.33 MeV with $\beta=0.211$. We found the $3^-$ state at 4.04 MeV with an assumed $\beta=0.20$ to have negligible effects for $s$ waves.

Using coupled channels we fitted with only minor changes in $V_0$ and $W_D$ (see Table I) to obtain curves almost identical to the spherical OMP curves in Fig. 2. This result is consistent with those shown in Table I for the lighter nuclei; in each case the inclusion of vibrational effects requires only minor changes in the well depths for $s$ waves. Further discussion is given in Sec. VII.

## IV. SCATTERING LENGTH $R'$ FOR $^{60}$Ni

In the literature $R'$ has generally been defined by Eq. (1) as a low energy limit. Ideally $R'$ should represent the effects of distant levels, but, being so defined, it can be distorted if a wide level lies just below zero energy. We avoid that uncertainty by using an energy-dependent definition,

$$R'(E)=\mathrm{Re}\delta(E)/k\ . \tag{14}$$

At the low energy limit this has the same uncertainties as the usual definition, but over most of the region of a measurement, particularly at the center, it has little uncertainty because the nearby levels are explicitly included in the analysis.

TABLE I. Model[a] potential well depths.[b]

| Target | $l$ | $V_0$ (MeV) sph | $V_0$ (MeV) cc | $W_D$ (MeV) sph | $W_D$ (MeV) cc | $V_{so}$ (MeV) sph | $V_{so}$ (MeV) cc |
|---|---|---|---|---|---|---|---|
| $^{30}$Si[c,d] | 0 | 48(1.7) | 49.5 | 2.0(1.5) | 1 | | 3.3[b] |
| | 1 | 62(2.5) | 51.5 | 4.5(2.5) | 2 | | 3.3[b] |
| $^{32}$S[e,f] | 0 | 51.5(0.4) | 50.8 | 6.0(3.0) | 4.0 | | 5.3 |
| | 1 | 61.4(1.1) | 50.8 | 2.7(1.5) | 0.8 | 11(3) | 5.3 |
| $^{34}$S[c,d] | 0 | 51.5(1.1) | 50.5 | 3.0(2.0) | 2.5 | | 3.5 |
| | 1 | 58.5(1.2) | 51 | 3.5(1.9) | 2.5 | 6(3.5) | 3.5 |
| $^{60}$Ni | 0 | 48(5) | 50 | 29(5) | 24 | | 5[g] |
| | 1 | 48[g] | 50[g] | 2.3(0.4) | 1.5 | 5[g] | 5[g] |

[a]Model geometric parameters are $r_0=r_D=1.21$ fm, $a_0=0.66$ fm, $a_D=0.48$ fm.
[b]Uncertainties for the spherical (sph) model are in parentheses. The same uncertainties apply to the coupled-channel (cc) model.
[c]See Ref. 8 for the spherical model.
[d]See Ref. 15 for the coupled channel model.
[e]See Ref. 7 for the spherical model.
[f]See Ref. 14 for the coupled channel model.
[g]Assumed well depth.

Figure 3 presents $R'$ for the various averages and models. Three of these curves are transformations from Fig. 2 with the same line symbols, i.e., the short-dash curve is for the numerical average with $I=90$ keV, the solid curve is the analytical approximation with $I=90$ keV, and the long-dash curve is for the models. A fourth curve (dash-dot) shows the analytical approximation for very large $I$. For the models, since $R'$ is nearly constant, the entire region can be treated as a low energy limit. Vertical bars are included on the dash-dot curve to show typical uncertainties propagated from Porter-Thomas fluctuations in the strength function. The error bar is smallest at the midpoint where the fluctuation effects for nearby external levels tend to cancel. At the midpoint we find $R'=5.5\pm0.03$ fm.

To make the connection to previously published values of $R'$, we first solve for $R'$ from Eq. (14) and the analytical approximation of Eq. (7) for large $I$,

$$R'(E)=a-\frac{1}{2k}\tan^{-1}\frac{\rho\tilde{R}(E)}{1-\pi\rho\tilde{s}}-\frac{1}{2k}\tan^{-1}\frac{\rho\tilde{R}(E)}{1+\pi\rho\tilde{s}}\ , \quad (15)$$

where $\rho=ka$. This equation gives the dash-dot curve in Fig. 3. Since the terms in $\tilde{s}$ have opposite signs, their effects tend to cancel, and the following often becomes a good approximation:

$$R'(E)=a-k^{-1}\tan^{-1}[\rho\tilde{R}(E)]\ , \quad (16)$$

Finally, if $\rho\tilde{R}$ is small because either $\rho$ or $\tilde{R}$ is small, we have

$$R'(E)=a[1-\tilde{R}(E)]\ . \quad (17)$$

In the literature, e.g., Ref. 1, one often finds the expression

$$R'=a(1-R^{\infty})\ , \quad (18)$$

which is similar to Eq. (17) except that $R^{\infty}$, unlike $\tilde{R}$, is related to the actual scattering function rather than to its average. The $R^{\infty}$ is defined to be a simple function, say linear in energy, which adequately describes $R^{\text{ext}}$, except possibly near the end points. It must increase with energy whereas $\tilde{R}$ need not. We conclude Eq. (18) is wrong in concept for the purpose of comparison to an OMP. Although its use yields a proper result if $R^{\infty}$ is evaluated at the center of the interval, it can also give a wrong answer if evaluated off center. For the present data, for example,

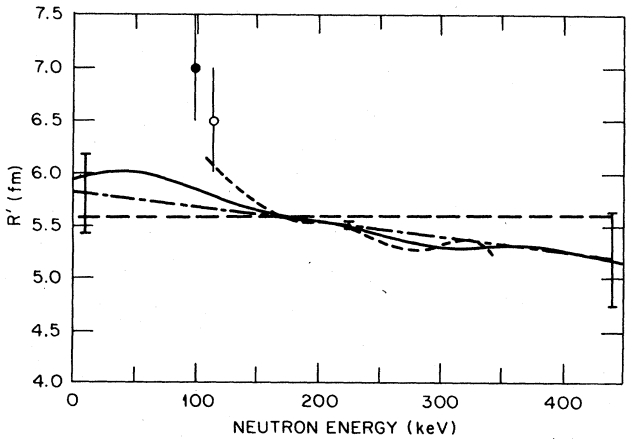


FIG. 3. Scattering length $R'$ vs neutron energy. (a) Short-dash curve, numerical average for $I=90$ keV; (b) solid curve, analytical for $I=90$ keV; (c) long-short dash curve, analytic for very large $I$; (d) long-dash curve, models. These line symbols [except (c)] are the same as in Fig. 1. Vertical bars on the long-short-dash line are uncertainties propagated from Porter-Thomas fluctuations in the strength function. Previous measurements are plotted at the midpoint of the previous data and are shown by an open circle (Ref. 17) and closed circle (Ref. 18).

a linear approximation to $R^\infty$ in Fig. 1 would intercept zero energy at about $-0.2$ and the resulting $R'$ from Eq. (18) would be 7.2 fm, in serious disagreement with the curves in Fig. 3 or with the midpoint value of 5.5 fm. In effect Eq. (18) has often been evaluated at the midpoint to give an approximate value for $R'$. In particular Firk, Lynn, and Moxon[16] emphasized that the calculation be done at the midpoint for proper comparison to the OMP.

Mughabghab *et al.*[1] evaluated $R'$ to be $6.7\pm0.3$ fm on the basis of two earlier measurements, a 1961 measurement ($6.5\pm0.5$ fm) by Bilpuch *et al.*[17] and a 1971 measurement ($7.0\pm0.5$ fm) by Stieglitz *et al.*[18] In both cases $^{60}$Ni transmissions were measured for about 0—200 keV neutrons and fitted by an approximate multilevel $R$-matrix equation. The values of $R'$ were deduced, essentially, from Eq. (18). In Fig. 3 we have plotted each result by a datum point at the midpoint of the analysis, even though it is not clear[17,18] that the evaluation was weighted toward the center. In Bilpuch's[17] analysis, for example, the $R^{\text{ext}}$ was set to zero and the radius $a$ was adjusted for best fit. Since $R^\infty$ must in fact increase with energy, the resulting fit had to be a compromise. If the compromise favors the middle region, the resulting $R'$ should be a good estimate, but if it favors the lower region, the $R'$ would be too large. In any case, both earlier values of $R'$ are significantly larger than deduced here from Perey's more recent data.[2]

## V. $p$ WAVES

Perey *et al.*[2] found the resonance structure of $^{60}$Ni too complicated for definitive conclusions about $p$-wave neutrons. Nevertheless, their listing of resonance energies and $g\Gamma_n$ for the many narrow resonances with $l>0$ does provide us with information on $\sigma_c$ because, even though some of the resonances have $l>1$, we can calculate an upper limit for the $p$ wave $\sigma_c$. This limit will not be far above the true value if we confine our calculations to the lower part of their energy region where the centrifugal barrier inhibits higher partial waves. Thus, assuming all of these resonances are $p$ waves in the limited region from 0 to 200 keV, we find $\tilde{s}_1=0.0092\pm0.0014$ for Perey's boundary condition or a conventional[1] strength of $S_1=(0.30\pm0.05)\times10^{-4}$ for a radius of $1.35A^{1/3}$ fm.

Following JLMW we average assuming $\tilde{R}=0$ (not critical) and find $\sigma_c=0.14\pm0.02$ b at the center energy of 100 keV. From our fitted $s$-wave OMP, assuming it applies to all even parity waves, we calculate the $d$-wave contribution to be only 20% of the observed value. So, we conclude $\sigma_c<0.14$ b for $p$ waves at 100 keV.

Even this upper limit on $\sigma_c$ is much smaller than predicted by the optical model which was deduced for $s$ waves in Sec. III. Therefore, following the method used[7,8,14,15] for the lighter nuclei in Table I, we assume a model with the given geometry but with different potentials for even and odd parities. Since $\sigma_c$ is small for $p$ waves, we expect $W_D$ for the odd potential to be relatively small.

For $p$ waves the $R^{\text{ext}}$ given by Perey[2] is not accurate enough for deducing $\sigma_{\text{se}}$ and for fitting with $V_0$. A possible assumption is that $V_0$ is the same for both even and odd potentials. For a spherical well, however, we see for the lighter nuclei in Table I that this is a bad assumption. For $^{60}$Ni there is additional evidence in that an odd parity model with $V_0=48$ MeV, as for $s$ waves, predicts the $3p$ size resonance to be at $A\simeq110$, in disagreement with the known[1] peak at $A\simeq95$. This difference is related to that in $V_0$ for the lighter nuclei. On the other hand, we see from Table I that the coupled-channel model removed the strong parity dependence for the lighter nuclei. Thus, it is reasonable to use the coupled-channel model with the assumption that $V_0$ has no parity dependence.

Using the coupled-channel model with an assumed parity-independent $V_0$ of 50 MeV, which is our fitted value for $s$ waves, we reduce the odd parity $W_D$ to 1.5 MeV in order to fit the observed 0.14 b limit in $\sigma_c$ for $p$ waves at $E_n=100$ keV. Here the effect of the $3^-$ state at 4.04 MeV ($\beta=0.2$) is not negligible; if it were omitted the $W_D$ would be reduced only to 2 MeV.

## VI. AVERAGED TOTAL CROSS SECTIONS FOR $^{60}$Ni

Figure 4 gives a comparison of averaged total cross sections, both model and experimental, for 0—2 MeV neutrons on $^{60}$Ni. The solid curve below 0.45 MeV is the sum of the $s$-wave experimental cross sections from Fig. 2 ($\sigma_c+\sigma_{\text{se}}$ for the analytic approximation) plus an estimated contribution for $l>0$. To estimate $\sigma_c$ for $l>0$ we calculated $2\pi^2k^{-2}\langle g\Gamma_n\rangle/D$ by averaging the observed[2] non-$s$-wave resonances in 100-keV intervals. (At 450 keV we corrected for missing levels.) To estimate $\sigma_{\text{se}}$ for $l>0$

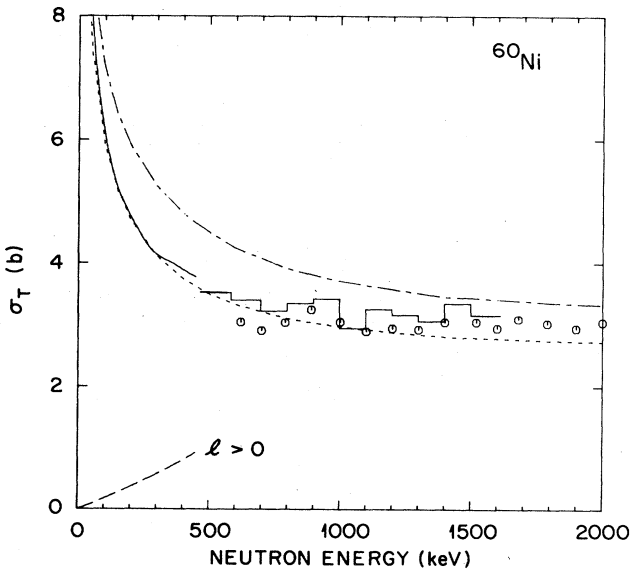


FIG. 4. Total cross section versus neutron energy. (a) Data points from Ref. 10; (b) histogram, current average of unpublished data of Ref. 2; (c) solid line, total cross section from present analysis; (d) long-dash curve, estimate for $l>0$; (e) short-dash curve, present coupled-channel model; (f) dash-dot curve, coupled-channel model of Guss *et al.*, Ref. 11.

we assumed only $p$ waves to be significant and to be given by that for a hard sphere of radius $1.35A^{1/3}$ fm. The long-dashed curve in Fig. 4 shows the estimated $l>0$ contribution; it is about 9% of $\sigma_T$ at 225 keV and 25% at 450 keV.

Above 450 keV the solid curve is continued by a histogram which we found by straightforward averaging of Perey's[2] high resolution cross sections. For comparison, the points in the figure show $\sigma_T$ deduced by Smith *et al.*[10] from poor-resolution transmission measurements with a thicker sample (0.18 atoms/b vs Perey's 0.074). As Smith *et al.* predicted, their points lie below the histogram at lower energies because of the nonlinear attenuation on the thicker sample. We also obtained a histogram (not shown) by the averaging of Perey's transmissions, rather than cross sections, and found values 3.5% lower at the low energy end and 0.3% lower at the high end. These discrepancies confirm that one must average cross sections rather than transmissions to avoid the nonlinear effects. The fact that the discrepancies are small indicates there are negligible remaining perturbations in the plotted histogram.

Figure 4 also includes curves for two coupled-channel models. The short-dash curve is for our parity-dependent model, as already discussed. At 2 MeV the curve falls below the observed cross sections. Therefore, this model, which was designed primarily for low energy $s$ waves, needs modification to describe the sum of all partial waves at higher energy. Smith *et al.*[10] came to a similar conclusion; they found OMP parameters which worked well above 2.5 MeV but gave too high cross sections at lower energies.

The dash-dot curve is calculated from the coupled-channel model of Guss *et al.*[11] They parametrized their model not only to fit their measured cross sections and analyzing powers for fast neutron (8, 10, 12, and 14 MeV) scattering to the ground and first excited states of $^{60}$Ni, but also to fit $S_0$, $S_1$, $R'$, and $\sigma_T$ at low energies. The fact that their model gives too high total cross sections in Fig. 4 probably results from the erroneously large $R'$, as shown in Fig. 3. Further discussion is given in the following.

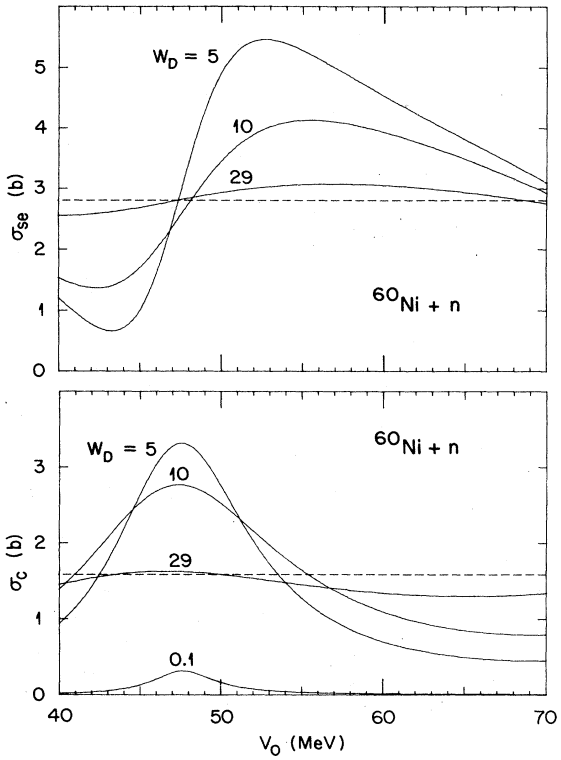


FIG. 5. Spherical OMP $s$-wave shape elastic and compound nuclear cross sections vs $V_0$ for various imaginary well depths at $E_n=200$ keV. The horizontal dotted lines indicate the experimental values.

## VII. DISCUSSION

### A. The importance of $\sigma_{se}$

A major thesis of our work is that the off-resonance neutron scattering, as expressed by a shape elastic cross section $\sigma_{se}$, plays a role in the parametrization of the OMP at least as important as the resonance scattering, as expressed either by a compound nucleus cross section $\sigma_c$ or a strength function. This dual importance was recognized by the early workers who measured low energy $s$-wave scattering and reported not only the strength function $S_0$ but also the potential scattering radius $R'$. Both quantities were important for the $s$-wave OMP. However, many recent measurements at higher energies and higher partial waves have been reported and interpreted only with respect to the strength functions.

For the spherical OMP the importance of simultaneous examination of both $\sigma_c$ and $\sigma_{se}$ for $s$-wave neutrons on $^{60}$Ni is demonstrated by Fig. 5, which shows these cross sections calculated for $E_n=200$ keV and plotted vs $V_0$ not only for the best fit $W_D$ of 29 MeV but also for three smaller values, namely, 0.1, 5.0, and 10 MeV. The measured cross sections at 200 keV are shown by horizontal dashed lines. The peak of the $3s_{1/2}$ single-particle resonance in $\sigma_c$ occurs near 47.5 MeV. As $W_D$ increases, the peak height first increases and then decreases as the $3s$ resonance broadens. The experimental $\sigma_c$ could be fit by a broad range of $W_D$ if there were no restrictions on $V_0$, but the experimental $\sigma_{se}$ restricts $V_0$ to about 48 MeV. Given the restrictions on $V_0$, one might expect a good fit to be achieved with small $W_D\simeq 0.5$ MeV. However, the resulting $\sigma_{se}$ would have a strong energy dependence, in disagreement with Fig. 2. Thus, only a rather large value of $W_D$ is acceptable and, finally, the best fit is achieved by $W_D=29$ MeV and $V_0=48$ MeV, each with $\pm 5$ MeV uncertainty. This $V_0$ is in good agreement with position of the $3s$ size resonance near $A=55$.

Figure 6 is similar to Fig. 5 but for the coupled-channel OMP with the $2^+$ (1.33 MeV) target state included. Again the $\sigma_c$ curve for $W_D=1.5$ shows the $3s_{1/2}$ resonance, but it is moved down about 2 MeV from the unperturbed energy in Fig. 5. In addition, particle-core resonances are seen near $V_0=55.5$ and 59.5 MeV, the first for $[2d_{5/2}\otimes 2^+]_{\frac{1}{2}}^+$ and the second $[2d_{3/2}\otimes 2^+]_{\frac{1}{2}}^+$. The ar-

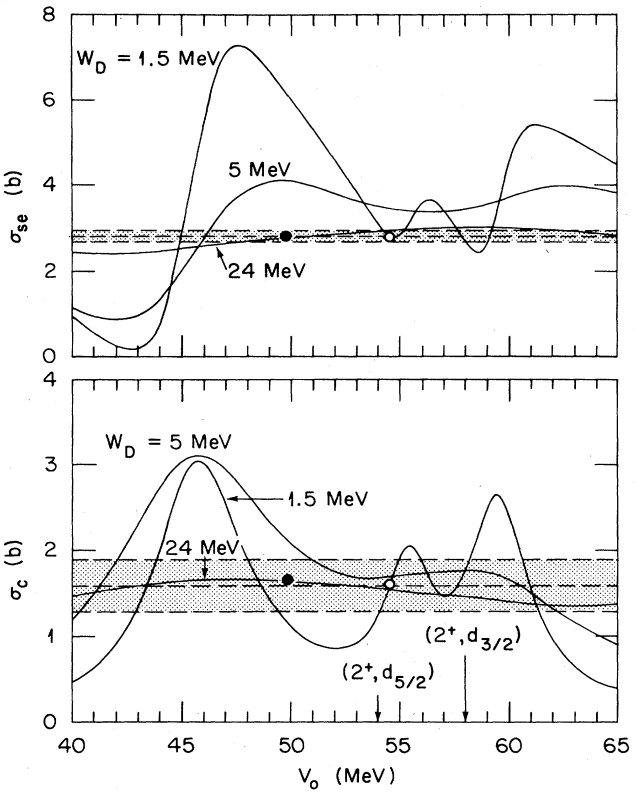


FIG. 6. Coupled channels OMP $s$-wave shape elastic and compound nuclear cross sections as for Fig. 5. The $2^+$ (1.33 MeV) target state is included with $\beta=0.211$. Arrows indicate unperturbed energies of the $[2^+, 2d_{5/2}]$ and $[2^+, 2d_{3/2}]$ particle-core states. Experimental uncertainties are indicated by the limits of the shaded areas. Solid points indicate the accepted model (Table I) and the open points indicate a rejected solution.

rows indicate the unperturbed resonance energies deduced by simple addition of the 1.33-MeV core energy to the $2d_{5/2}$ and $2d_{3/2}$ binding energies for the model obtained using the real potential well $V_0$ vs $V_{so}$. That is, the arrows indicate where $E_{s.p.}(V_0)+E(2^+)=200$ keV. This clearly identifies the source of the resonances. A plot of $\sigma_c$ vs $V_0$ is equivalent to a plot[1] of the $s$-wave strength function vs $A$. The shoulder in the strength function curve for values of $A$ between 75 and 85, which is reproduced by the original coupled channels calculation of Buck and Perey,[19] is a manifestation of the resonances due to $d$-wave coupling to the $2^+$ state as exhibited in Fig. 6.

The shaded regions in the figure indicate the limits of experimental uncertainties propagated primarily from the $\pm 25\%$ uncertainty in the strength function. As for the spherical model we adjusted $W_D$ and $V_0$ to obtain a fit as shown by the solid symbols with $V_0=50$ MeV and $W_D=24$ MeV, each with $\pm 5$ MeV uncertainty.

The open symbols in Fig. 6 indicate an equally acceptable fit is obtained with $V_0=54.4$ MeV and $W_D=1.5$ MeV, each with small uncertainty. That model has desirable features in that it gives a reasonably small $W_D$ and does not require an $l$ dependence to fit $p$ waves. Nevertheless, we do not choose this solution because the $V_0$ is too large to satisfy other factors. Firstly, for this $V_0$ the peak of the $3s$ size resonance is predicted at $A=44$, in contradiction to the known position near $A=55$. Secondly, the bound $2p$ states in $^{61}$Ni are predicted at $-10.8$ MeV for $p_{3/2}$ and $-9.5$ MeV for $p_{1/2}$, in disagreement with the experimental[20] energies of $-7.8$ and $-7.5$ MeV. In contrast, our model with $V_0=50$ MeV binds these states at $-8.1$ and $-6.8$ MeV, in reasonable agreement with the known values. We also note that the $V_0$ of 50 MeV is consistent with the values for other nuclei in Table I.

Essentially the model of Guss *et al.*,[11] which we discussed relative to Fig. 4, corresponds to this alternate solution. Figure 7 shows curves very similar to Fig. 6 except that the model geometry is that of Guss *et al.* The primary difference between the two figures is a shift in resonance energies which results from different real potential radii, $1.21A^{1/3}$ vs $1.165A^{1/3}$. The solid symbols represent the solution by Guss *et al.* and the open points indicate appropriate adjustments to fit the present analysis of Perey's data. The resulting $V_0$ of 58 MeV for 0.2-MeV neutrons would require an energy coefficient of 0.62 MeV$^{-1}$ rather than their value of 0.46 MeV$^{-1}$ to restore their potential at about 11 MeV. These modified parameters result in a reasonable fit to the $\sigma_T$ in Fig. 4.

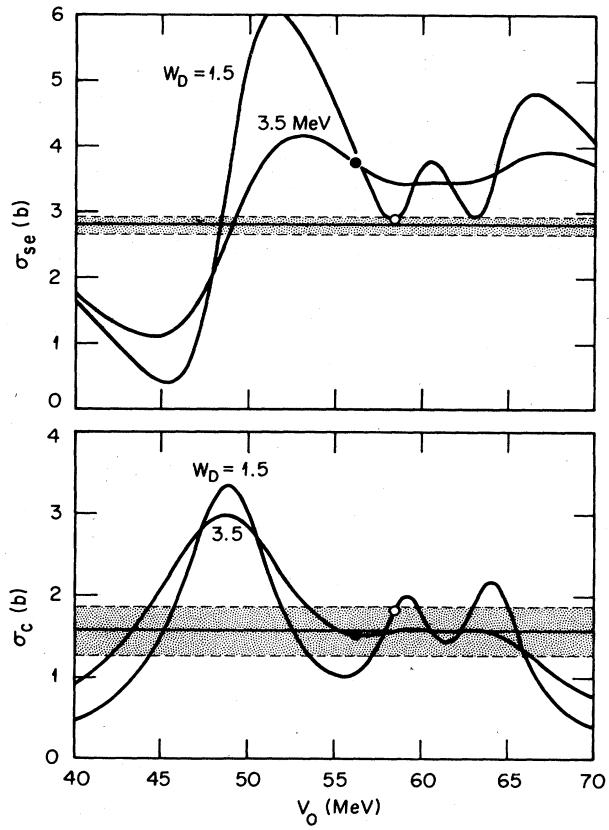


FIG. 7. Coupled channels OMP $s$-wave shape elastic and compound nuclear cross sections as for Fig. 6. The geometrical parameters and $V_{so}$ of Ref. 11 were assumed. The solid points indicate the OMP parameters from Ref. 11 and the open points show the modified parameters for fitting within the experimental shaded limits.

Nevertheless, we do not choose these parameters for the same reason that we did not choose the equivalent solution ( $V_0 = 54.4$ MeV) with our geometry.

Our choice of a model with a large $W_D$ rather than a large $V_0$ is a matter of judgment. It is reasonable that nuclear structure effects in this mass region could be producing an $A$ dependent absorption strength similar to that previously found in the mass 100 region for both proton[21] and neutron[22] scattering.

For the coupled-channel model the $s$-wave real well depths for the four nuclei in Table I agree well within the experimental uncertainties. The agreement is almost as good for the spherical model. These results came primarily from the data on $\sigma_{se}$ for $s$ waves. From corresponding data on $p$ waves, which are available only for the three lighter nuclei, the real well is seen to be $l$ dependent for the spherical model,[7,8] but not for the coupled-channel models.[14,15]

### B. $l$ dependence of $W_D$

Since we do not have experimental data on $\sigma_{se}$ for both $s$ and $p$ waves we made the above-mentioned reasonable assumption that $V_0$ is parity independent for the coupled-channel OMP and found $W_D^-$ for the odd parity potential to be 1.5 MeV, much smaller than $W_D^+ = 24$ MeV for even parities. The current form of the coupled channels code used,[13] ECIS79, allows for the use of parity but not $l$-dependent potentials. Therefore we use the terms $l$ dependent and parity dependent interchangeably. Hence, in this model, the $\frac{1}{2}^-$ and $\frac{3}{2}^-$ compound states do not arise from spreading of the bound $2p$ states or from coupling of the odd parity states with the $2^+$ core, but primarily from coupling of the $3^-$ core with broadened states in the even parity potential. The coupled configurations are the $(2d, 3^-)$ particle-core states, which are unbound by about 5 MeV but are widely spread by the $W_D^+$ potential of 24 MeV.

This conclusion is physically reasonable. It means that the deeply bound odd parity states are not fragmented as are the unbound states. But such a hypothesis is preliminary; data with analyses on other nuclei are needed. Preliminary analyses suggest the same phenomenon for $^{40}$Ca (Ref. 23) and $^{187}$Os (Ref. 24). A reversal in the parity roles would be expected for the mass $\approx 100$ region, for which the even states are bound and the odd unbound. This corresponds to a region with minimum $s$-wave and maximum $p$-wave strength functions.[1] Some preliminary evidence for this phenomenon shows up in $^{120}$Sn.[24]

A study of other possible model geometries could be made. Moldauer[25] introduced a potential with the absorptive radius placed 0.5 fm outside the real radius and with a small diffuseness equivalent to $a_D = 0.23$ fm. Using that geometry and a parity-independent $V_0$ for the spherical model, we found $W_D = 35$ MeV for $s$ waves and 9 MeV for $p$ waves. Possibly the present data on $s$ and $p$ waves could be fit without parity dependence if a very narrow absorptive potential were placed at the node of the wave function for $p$ waves, as discussed by Moldauer. Since such a potential would predict a narrow minimum at $A = 60$ in a plot of $S_1$ vs mass, it also would need more study for other nuclei such as $^{40}$Ca.

## ACKNOWLEDGMENTS

We are indebted to Dr. D. J. Horen for helpful discussions. This research was sponsored by the Division of Basic Energy Sciences, U.S. Department of Energy, under Contract No. DE-AC05-84OR21400 with the Martin Marietta Energy Systems, Inc. and No. DE-AC02-76-ER02696 with Denison University.

[1] S. F. Mughabghab, M. Divadeenam, and N. E. Holden, *Neutron Cross Sections* (Academic, New York, 1981), Vol. 1, Part A.

[2] C. M. Perey, J. A. Harvey, R. L. Macklin, F. G. Perey, and R. R. Winters, Phys. Rev. C **27**, 2556 (1983).

[3] C. H. Johnson, N. M. Larson, C. Mahaux, and R. R. Winters, Phys. Rev. C **27**, 1913 (1983).

[4] W. M. MacDonald and M. C. Birse, Nucl. Phys. **A403**, 99 (1983).

[5] W. M. MacDonald and M. C. Birse, Phys. Rev. C **29**, 1560 (1984).

[6] C. H. Johnson, N. M. Larson, C. Mahaux, and R. R. Winters, Phys. Rev. C **29**, 1563 (1984).

[7] C. H. Johnson and R. R. Winters, Phys. Rev. C **27**, 416 (1983).

[8] R. F. Carlton, J. A. Harvey, and C. H. Johnson, Phys. Rev. C **29**, 1988 (1984).

[9] Analysis of unpublished data of Perey *et al.* (Ref. 2).

[10] A. Smith, P. Guenther, D. Smith, and J. Whalen, Nucl. Sci. Eng. **72**, 293 (1979).

[11] P. P. Guss, R. C. Byrd, C. E. Floyd, C. R. Howell, K. Murphy, G. Tungate, R. S. Pedroni, R. L. Walter, J. P. Delaroche, and T. B. Clegg, Nucl. Phys. (to be published).

[12] T. Tamura, Rev. Mod. Phys. **37**, 679 (1965).

[13] J. Raynal, ECIS79 (private communication); the present version was modified by R. L. Hershberger to print partial wave quantities.

[14] A. D. MacKellar and B. Castel, Phys. Rev. C **28**, 441 (1983).

[15] A. D. MacKellar and B. Castel, Phys. Rev. C **29**, 1993 (1984).

[16] F. W. K. Firk, J. E. Lynn, and M. C. Moxon, Proc. Phys. Soc. (London) **82**, 477 (1963).

[17] E. G. Bilpuch, K. K. Seth, C. D. Bowman, R.H. Tabony, R. C. Smith, and H. W. Newson, Ann. Phys. (N.Y.) **14**, 387 (1961).

[18] R. C. Stieglitz, R. W. Hockenbury, and R. C. Block, Nucl. Phys. **A163**, 592 (1971).

[19] B. Buck and F. Perey, Phys. Rev. Lett. **8**, 444 (1962).

[20] R. L. Auble, Nucl. Data Sheets **16**, 1 (1975).

[21] C. Johnson, A. Galonsky, and R. Kernell, Phys. Rev. C **20**, 2050 (1979); R. Hershberger, D. Flynn, F. Gabbard, and C. Johnson, *ibid.* **21**, 896 (1980); D. Flynn, R. Hershberger, and F. Gabbard, *ibid.* **26**, 1744 (1982).

[22] A. B. Smith, P. J. Guenther, and J. F. Whalen, Nucl. Phys. **A415**, 1 (1984).

[23] A. D. MacKellar and C. H. Johnson (unpublished).

[24] M. T. McEllistrem and J. L. Weil, private communication.

[25] P. A. Moldauer, Nucl. Phys. **47**, 65 (1963).